Enhanced nitrogen diffusion induced by atomic attrition

E. A. Ochoa, C. A. Figueroa, T. Czerwiec [a], and F. Alvarez [b]

Instituto de Física "Gleb Wataghin", Universidade Estadual de Campinas, Unicamp

13083-970, Campinas, São Paulo, Brazil

The nitrogen diffusion in steel is enhanced by previous atomic attrition with low energy xenon ions. The noble gas bombardment generates nano-scale texture surfaces and stress in the material. The atomic attrition increases nitrogen diffusion at lower temperatures that the ones normally used in standard processes. The stress causes binding energy shifts of the Xe $3d_{5/2}$ electron core level. The heavy ion bombardment control of the texture and stress of the material surfaces may be applied to several plasma processes where diffusing species are involved.

[a)] Laboratoire de Science et Genie des Surfaces, (UMR CNRS 7570), Institut National Polytechnique de Lorraine, Ecole des Mines de Nancy, Parc de Saurupt, 54042 Nancy Cedex, France.

[b)] Corresponding address: alvarez@ifi.unicamp.br

PACS : 66.30.-h ; 68.35.Fx ; 68.35.Gy

The properties of materials obtained in several applications involving plasma such as plasma enhanced deposition, ion beam assisted deposition, pulsed plasma nitriding are directly influenced by the defects at the surface created by the impact of ions. Modern plasma nitriding combines low energy nitrogen ion implantation and posterior thermal diffusion [1,2]. Plasma nitriding is a broadly used thermo-chemical diffusion process increasing hardness, corrosion resistance, and improving tribological properties of iron based alloys. However, diminishing the relative long processing times continues to be a challenge for increasing applications of the process. The synergy between low energy ions and substrate temperature influencing kinetic surface phenomena recently demonstrated is an important route of working to decrease process time [3]. Mechanical attrition ("shot-peening") generating plastic deformation and defects modify the surface chemical kinetic of the reactions, shortening nitriding process by increasing boundary paths obtained in the nano-structured surface. [4, 5, 6, 7]. Recently, Abrasonis, Möller, and Ma showed nitriding enhancement in steel by ion argon pos-bombardment treatments. [8] These researches proposed a mechanism involving nonlinear elemental vibration excitation as the cause of the observed phenomenon.

In this letter we report that the preparation of the surface samples by low energy xenon ion bombardment ("atomic attrition") and posterior *in situ* nitriding process notably enhances nitrogen diffusion. This result allows lowering temperature process or shortening nitriding times, two important variables. Although less intense, similar results were obtained using krypton ions. In this paper, however, we shall focus the discussion on the experiments performed with Xe^+ bombardment. *In situ* photoemission electron spectroscopy (XPS) shows that the low energy (from 50 to 350 eV) implanted Xe^+ generate local stress ("atomic peening") [9, 10]. The local stress was studied investigating the binding energy shifts of the Xe $3d_{5/2}$ electron core level due to the pressure exerted on the trapped noble gas by the host crystalline structure. *Ex situ* scanning electron microscopy (FEG-SEM) shows that the Xe^+ bombardment generates nanometric fine grains at the material surface, augmenting diffusion paths. *Sputtered Neutral Mass Spectroscopy* (SNMS) shows enhancing nitrogen diffusion in previously Xe^+ bombarded substrates. Grazing angle difractograms show a remarkable increasing of species rich in nitrogen. These physical modifications lead to a more efficient nitriding process, increasing the material hardness. Finally, our findings combined with the results reported by Abrasonis and Möller suggest that the effect of bombarding the material before as well as after nitriding have profound consequences on N diffusion in metals. [8]

The experiments were performed in mirror polished, rectangular samples, 20 x 10 mm, 1mm thick, prepared from the same commercial AISI 4140 steel lot (C: 0.4, Si: 0.25, P:<0.04, S:<0.04, Mn: 0,85, Mo: 0.20, Cr: 1, Fe: balance). The Xe^+ implantation and nitriding experiments were carried out in a high-vacuum system ($<10^{-7}$ mbar) attached to an ultra high vacuum chamber ($<2x10^{-9}$ mbar) for XPS analysis. The deposition chamber contains a 3 cm

diameter DC Kaufman ion source. Details of the apparatus are described elsewhere [11]. Before nitriding, the surface of the samples is nano structured by Xe^+ bombardment during 30 minutes at room temperature with energies varying between 50 to 350 eV and ion current density of 1mA/cm^2. Immediately, the substrate temperature is raised to the working nitriding temperature (380+/-5)^{o}C in approximately 15 minutes. Subsequently, the sample is irradiated with a pure nitrogen ion beam of 1 mA/cm^2 and constant energy (200 eV) for all the studied samples. Two sets of samples were prepared by irradiating the substrate during 30 minutes and 120 minutes, respectively. The treated sample is then transferred to the XPS analysis chamber. The hardness profiles were obtained by nano- indentation using a Berkovich diamond tip (*NanoTest-300*) and the load-displacement curves were analyzed by the Oliver and Pharr method [12]. The nitrogen profiles were obtained from SNMS. The nitrogen concentration was obtained using a γ'-Fe_4N standard sample. The sample cross-section morphology was studied by FEG-SEM (ten second attack with a 5% Nital solution). The crystalline structure was studied by normal and glazing x-ray experiments. Numerical simulation using TRIM shows that the Xe depth in the studied samples varies between ~5 to 40 Å depths [13]. This is the region probed by the XPS technique [14]. The [Xe]/[Fe] ratio in all treated samples is ~1.3 +/-0.1 at % as obtained by XPS.

Figure 1(a) shows the hardness profiles of the nitrided samples *in identical conditions* but different Xe^+ bombarding preparation of the substrates. For comparison purposes, the hardness profiles of a sole Xe^+ bombarded (non nitrided) and raw samples are displayed. The increasing hardness at the surface of the raw material is explained by the bond order loss at the boundary sample and the polishing procedure [15]. Figure 1(a), inset, shows results obtained for longer nitriding time. Figure 1(b) shows the nitrogen profile obtained by SNMS of two nitrated samples with and without bombardment (125 eV Xe^+). Figure 1(b), inset, shows a linear relationship between hardness and nitrogen concentrations of these two samples [16]. Figure 1(a) shows a small hardness increasing in the sample treated (only) with Xe^+. TRIM simulation shows that the ion penetration for Xe 125 eV ions is ~10 Å (not shown). Therefore, the dislocations and defects causing the hardness increment propagate as far as ~700 nm. This "long range" phenomenon is a known effect [17]. The preparation of the substrate by Xe^+ bombardment enhances nitrogen diffusion efficiency, increasing hardening (Figure 1). For relative short nitriding time (0.5 hr), the curves for 125 and 300 eV are overlapping. Increasing nitriding time splits the hardness curves (Figure 1a, inset).

Figure 2 shows the grazing angle difractograms obtained in a selected group of studied samples. The peak associated with ε-$Fe_{2-3}N$ nitrides confirms the increasing retention of nitrogen at the surface in Xe^+ bombarded samples. Bulk difractograms (not shown) indicate the formation o γ′-Fe_4N and ε-$Fe_{2-3}N$ phases, confirming N deeper diffusion. Assuming a diffusion parabolic law, the ~8 GPa hardness, for instance, could be reached approximately

nine times faster by previous atomic attrition of the substrate (Figure 1) [18]. The shifting of the diffraction peak is probably due to the network distortion occasioned by the ion bombardment (stress).

The Xe/Fe atomic ratio size is ~ 1.7. In the same units, the size of the largest α(bcc) interstitial site in Fe is ~ 0.37 (tetrahedral) and 0.19 (octahedral), respectively [19]. Let us assume for simplicity that, after few collisions, the Xe atoms occupy an interstitial site in the α (bcc) host crystal, causing stress. The increasing volume in the plane of the nitrided layer is prevented to expand due to the stiffness of the substrate [20, 21]. Therefore, due to the pressure caused by the misfitting atoms in the host crystal, the binding energy (BE) of the Xe $3d_{5/2}$ electron changes [22, 23]. Our results show BE changes of the Xe $3d_{5/2}$ core level up to -5 eV compared to the value measured in the free Xe atom (gas). This BE shift stems from the initial and final electronic state of the photo-ejected electron [22,24]. The initial state contribution to the BE shift is essentially due the increasing electron repulsion introduced by the compression of the electronic cloud charge. The final state contribution to the BE shift relies on the network relaxation energy (RE) due to the hole left behind by the photo-ejected electron. Therefore, subtracting the RE from the Xe $3d_{5/2}$ peak energy shift will provide the true energy, ΔE, associated with the Fe host crystal compression effect on Xe. Experimentally, the RE can be obtained using the Auger parameter, α [23,25,26]. Briefly, the Auger parameter is determined by α = K+BE, where K and BE are the kinetic energy of the Auger electron and the binding energy of the considered electronic level, respectively. The RE is then determined by the expression RE ≈ α/2 (14). Figure 3 shows the energy shift ΔE of the Xe $3d_{5/2}$ electron core level energies (after subtracting the RE) vs. the ion implantation energy of the studied samples. As observed, a local maximum occurs at ~125 eV. Above this energy, the energy shift diminishes due to plastic relaxation of the material. A similar curve with a maximum located at ~150 eV is obtained bombarding with Kr atoms (not shown). In this case, however, the maximum shift of the Kr $3p_{3/2}$ electron core level is around 25 % less than the shift obtained with the Xe $3d_{5/2}$ electron core level energy.

Fig. 4(a) shows the morphology of the nitrided layer *without* Xe^+ bombardment. The structural modification reaches up to 2 μm depth with lamellar precipitates. The detail (left) shows 60 to 130 nm size characteristic structures. The refining grain up to nanometric scale by Xe^+ bombardment creates numerous alternative paths for nitrogen diffusion (Fig. 4 b) [27, 28]. The micrograph of the nitrided Xe^+ bombardment sample shows a pattern formed by larger lamellar nitrogen precipitates, deeper in the sample, than the ones observed in Figure 4 (a), effect induced by the Xe^+ bombardment (Fig. 4(c)).

In conclusion, the preparation of the surface material by Xe^+ bombardment enhances nitrogen diffusion by grain refining up to nano-metric dimensions. Therefore, the nitriding time is shortened and the process temperatures

reduced. The atomic attrition generates stress as a consequence of the energy transferred by the impact and occupancy of small spaces by the massive Xe^+ ions (misfitting). Even though less intense, similar effects are observed using Kr^+.

Acknowledgments

This work was partially sponsored by Fapesp. FA is CNPq fellow. EAO and CAF are Fapesp fellows. The authors are indebted to H. Michel and E. J. Mittemeijer for critical reading of the manuscript. This work is part of the EAO PhD dissertation.

References

[1] R. Wei, Surf. Coat. Technol. 83, 218 (1996).

[2] T. Czerwiec, H. Michel, and E. Bergman, Surf. Coat. Technl., 108-109, 102 (1998); Rie, K. T., Menthe, E., Matthews, A., & Legg, K. Chin., J. *MRS Bulletin*, 46-51, August 1966.

[3] Z. Wang and E. G. Seebauer, Phys. Rev. Letters, 95, 015501 (2005).

[4] W. P. Tong, N. R. Tao, Z. B. Wang, J. Lu, K. Lu, *Science*, 299, 686 (2003).

[5] C. C. Koch, Nanostruct. Mater. 2, 109 (1993).

[6] C. Suryanarayana, Prog. Mater. Sci. 46, 1 (2001).

[7] Q. Jiang, S. H. Zhang, J.C. Li, Sol. Stat. Comm. 130, 581(2004).

[8] G. Abrasonis, W. Möller, and . X. Ma, Phys. Rev. Letters 96, 065901-1 (2006).

[9] C. A. Davis, Thin Sol. Films, 226, 30 (1993).

[10] H. Windischmann, J. Appl. Phys. 62, 1800 (1987).

[11] P. Hammer, N. M. Victoria, and F. Alvarez, J. Vac. Sci. Technol. A 16, 2941 (1998).

[12]W. C. Oliver, and G. M. Pharr, J. Mater. Res. **7**, 1564 (1992).

[13] J. P. B. Biersack, and G. L. Haggmark, The simulation used the TRIM software, Nucl. Instrum. Methods **174**, 257 (1980).

[14] See *Practical Surface Analysis,* Second Ed., Vol. 1. Edited by D. Briggs and M. P. Seah, J. Wiley, New York, 1996.

[15] C. Q. Sun, W. H. Zhon, S. Li, and B. K. Tay, J. Phys. Chem. B, 108, 1080-1084 (2004).

[16] E. A. Ochoa, C. A. Figueroa, and F. Alvarez, Surf. & Coat. Technology, 200, 7, 2165 (2005).

[17] Yu. P. Sharkeev and E. V. Kozlov, Surf. And Coat. Technol. 158-159, 219 (2002), and references therein.

[18] W. D. Callister, Jr., *Materials Science and Engineering. An Introduction*, Fifth Ed., John Wiley & Sons, Inc., New York (2000).

[19] R. W. K. Honeycombe and H. K. D. H. Bhadeshia, *Steels, Microestructure and Properties*, Edward Arnold Publisher, London (1995).

[20] J. D. Kamminga, Th. H. de Keijser, and R. Delhez, J. Appl. Phys., 11, 6332 (2000).

[21] J.-D. Kamminga, Th. H. de Keijser, and R. Delhez, and E. J. Mittemeijer, Thin Sol. Films 317, 169 (1998).

[22] P. H. Citrin and D. R. Haman, Phys. Rev. B 10, 4948 (1974).

[23] R. G. Lacerda, M. C. dos Santos, L. R. Tessler, P. Hammer, F. Alvarez, and F. C. Marques, Phys. ReV. B 68, 54104-1 (2003).

[24] Y.Baba, H. Yamamoto and T.A. Sasaki, Surf. Science, 287/288 806 (1993).

[25] C. D. Wagner, Faraday Discuss. Chem. Soc. 60, 291 (1975).

[26] G. Moretti, J. Electron Spectrosc. Relat. Phenom. 95, 95 (1998).

[27] R. E Reed-Hill, *Physical Metallurgy Principles*, Second Ed., D. van Nostrand Company, New York, (1973).

[28] Q. Jiang, S. H. Zhang, J. C. Li, Sol. State Comm., 130 581 (2004).

Figure Captions

Fig. 1.(a) Hardness vs. depth. Crosses: raw material. Dots: sample sole bombarded with Xe^+ ions. Squares: nitrided samples without Xenon bombardment pre-treatment. Triangles and diamonds: nitrided samples pre-treated with X^+. The energies of the Xenon ions are indicated. Inset: Hardness vs. depth of nitrided samples pre-treated with Xe^+ and longer process time. (b) Nitrogen depth profile of two nitrated samples with and without bombardment of 125 eV Xe^+. Inset: hardness vs. N concentration of the same samples. The nitriding times are indicated.

Fig. 2. Grazing angle difractograms of the peak associated to ε-$Fe_{2-3}N$ of nitrided samples. The bombardment Xe^+ energies are indicated.

Fig. 3. Experimental binding energy shifts ΔE of the Xe $3d_{5/2}$ electron core levels (relative to the gas phase) minus the relaxation energy (RE) of the system vs. implantation energy.

Fig. 4. (a) SEM micrograph showing, the nitrided layer in a substrate without Xe^+ pre-implantation; (b) surface refinement due to the Xe^+ bombardment (125 eV); and (c) nitrided sample in a sample Xe^+ pre-implanted.

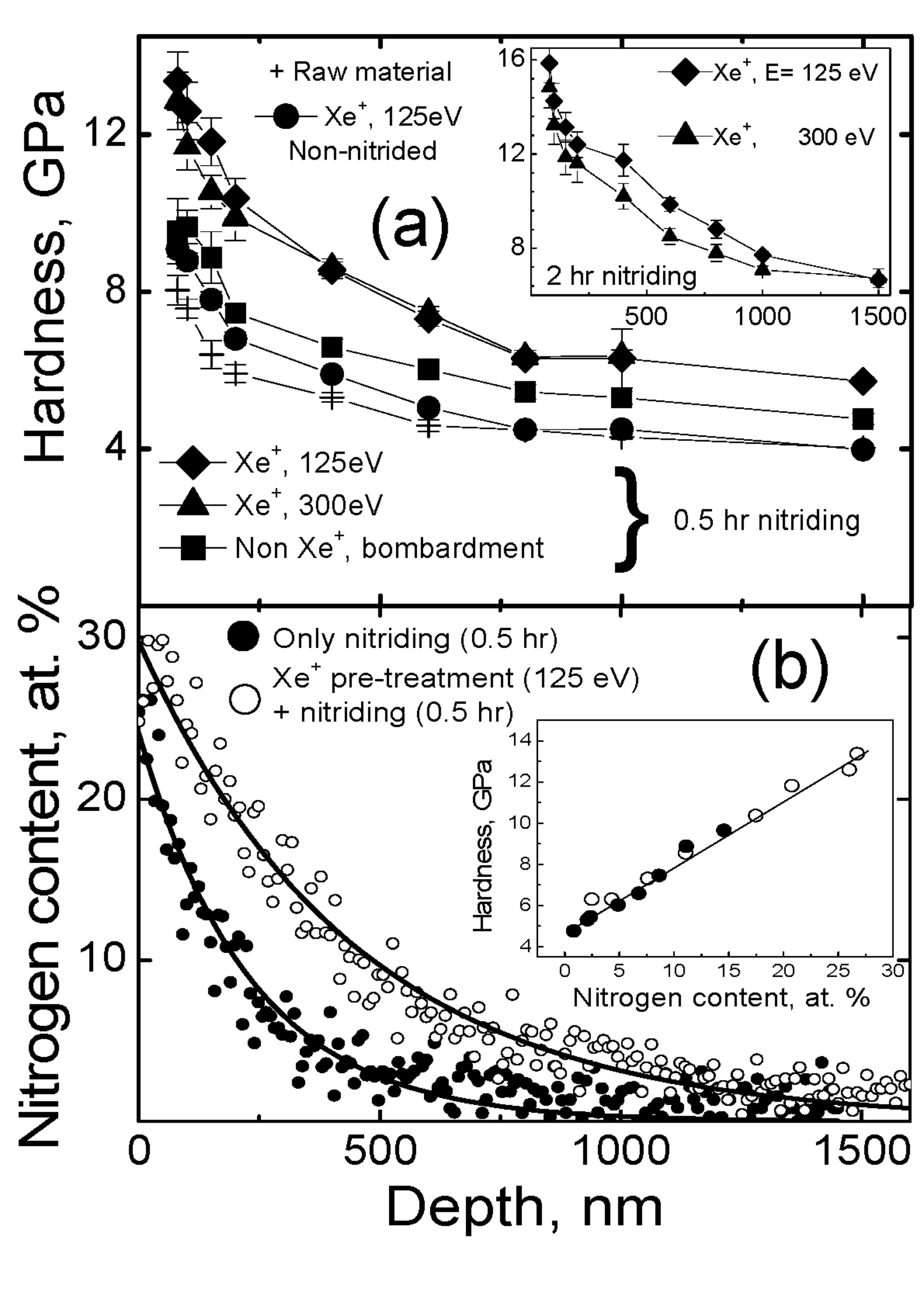
Hardness, GPa
+ Raw material
Xe+, 125eV
Non-nitrided
(a)
Xe+, E= 125 eV
Xe+, 300 eV
2 hr nitriding
Xe+, 125eV
Xe+, 300eV
Non Xe+, bombardment
0.5 hr nitriding
Nitrogen content, at. %
Only nitriding (0.5 hr)
Xe+ pre-treatment (125 eV)
+ nitriding (0.5 hr)
(b)
Hardness, GPa
Nitrogen content, at. %
Depth, nm

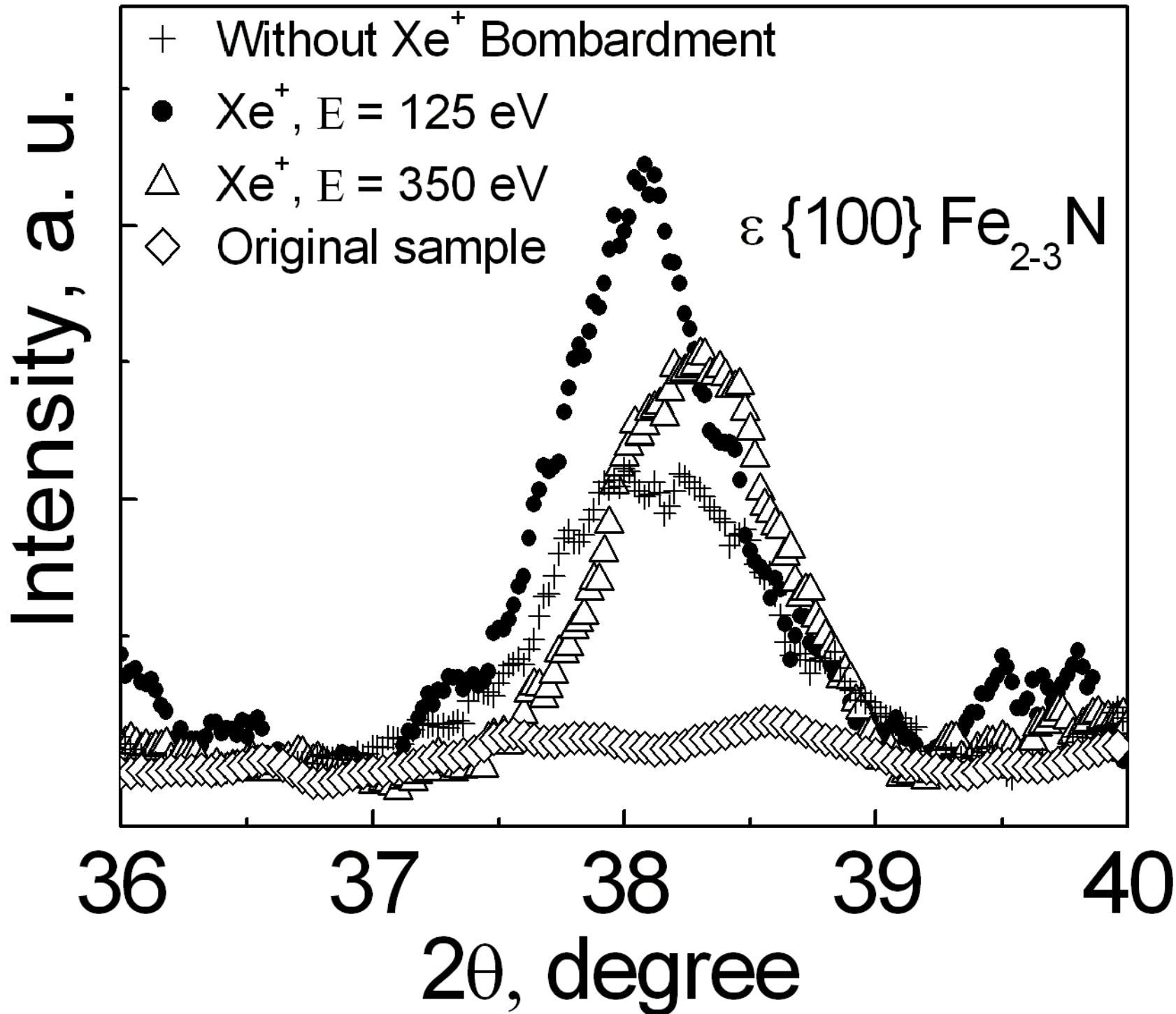
Without Xe+ Bombardment
Xe+, E = 125 eV
Xe+, E = 350 eV
Original sample
ε {100} Fe2-3N
Intensity, a. u.
36
37
38
39
40
2θ, degree

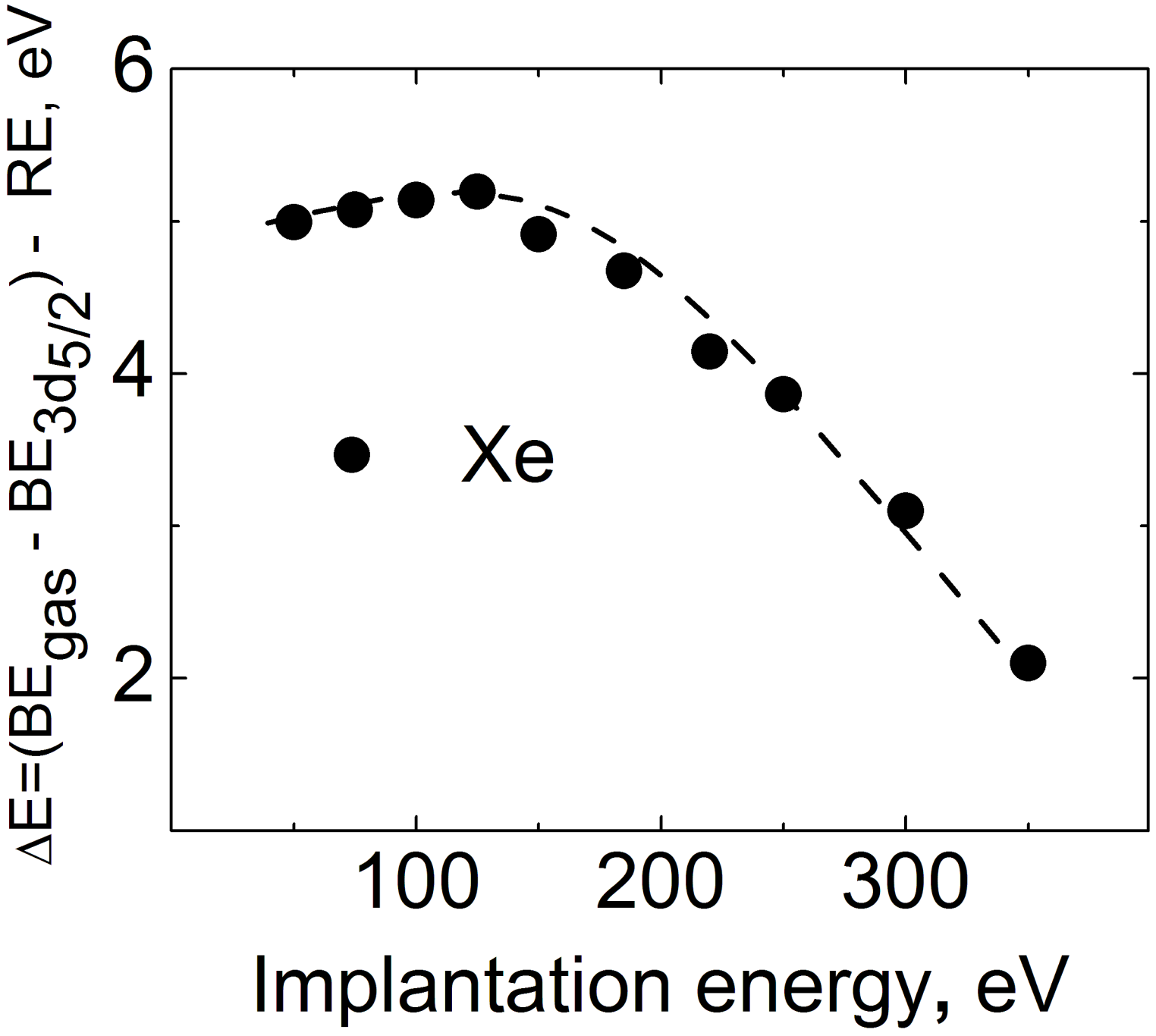
ΔE=(BE_gas - BE_3d5/2) - RE, eV
6
4
2
Xe
100
200
300
Implantation energy, eV

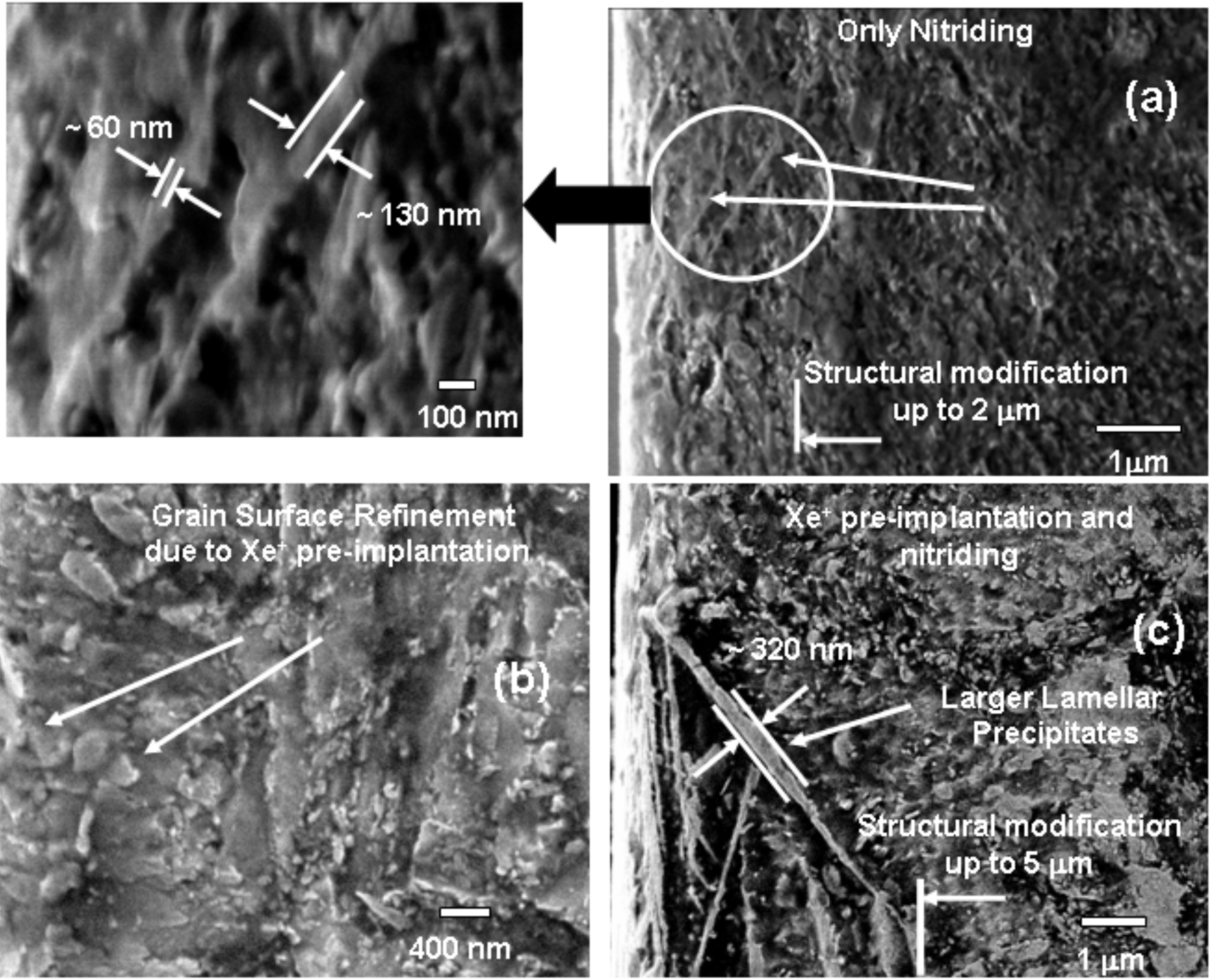
~ 60 nm
~ 130 nm
100 nm
Only Nitriding
(a)
Structural modification
up to 2 μm
1μm
Grain Surface Refinement
due to Xe+ pre-implantation
(b)
400 nm
Xe+ pre-implantation and
nitriding
(c)
~ 320 nm
Larger Lamellar
Precipitates
Structural modification
up to 5 μm
1 μm